

Primary structural dynamics in graphite

This article has been downloaded from IOPscience. Please scroll down to see the full text article.

2011 New J. Phys. 13 063030

(<http://iopscience.iop.org/1367-2630/13/6/063030>)

View [the table of contents for this issue](#), or go to the [journal homepage](#) for more

Download details:

IP Address: 141.89.199.236

The article was downloaded on 03/04/2012 at 19:14

Please note that [terms and conditions apply](#).

Primary structural dynamics in graphite

Sascha Schäfer, Wenxi Liang and Ahmed H Zewail¹

Physical Biology Center for Ultrafast Science and Technology,
Arthur Amos Noyes Laboratory of Chemical Physics,
California Institute of Technology, Pasadena, CA 91125, USA
E-mail: zewail@caltech.edu

New Journal of Physics **13** (2011) 063030 (9pp)


Received 9 April 2011

Published 17 June 2011

Online at <http://www.njp.org/>

doi:10.1088/1367-2630/13/6/063030

Abstract. The structural dynamics of graphite and graphene are unique, because of the selective coupling between electron and lattice motions and hence the limit on electric and electro-optic properties. Here, we report on the femtosecond probing of graphite films (1–3 nm) using ultrafast electron crystallography in the transmission mode. Two time scales are observed for the dynamics: a 700 fs initial decrease in diffraction intensity due to lattice phonons in optically dark regions of the Brillouin zone, followed by a 12 ps decrease due to phonon thermalization near the Γ and K regions. These results indicate the non-equilibrium distortion of the unit cells at early time and the subsequent role of long-wavelength atomic motions in the thermalization process. Theory and experiment are now in agreement regarding the nature of nuclear motions, but the results suggest that potential change plays a role in the lateral dynamics of the lattice.

 Online supplementary data available from stacks.iop.org/NJP/13/063030/mmedia

¹ Author to whom any correspondence should be addressed.

Contents

1. Introduction	2
2. Experimental details	3
3. Results and discussion	4
4. Conclusion	7
Acknowledgments	8
References	8

1. Introduction

In graphite, graphene and carbon nanotubes, the electron subsystem is strongly coupled to a small subset of optical phonons [1, 2]. The dynamics of these phonons and their interaction with the electron and other lattice modes are of interest not only on a fundamental level, but also because they play an essential role in the electric conduction properties of these carbon-layered materials [3, 4]. In the case of carbon nanotubes, it was shown that strongly coupled optical phonons (SCOP) limit the electric current at high bias voltage due to their incomplete equilibration with the remaining lattice bath [5].

The generation and decay of SCOP have been investigated with time-resolved optical transmission [6–9], THz [1] and photoluminescence spectroscopy [3, 10]. It was concluded that electrons thermalize with SCOP on a 100 fs time scale and that SCOP decay with a time constant of ~ 2 ps. The equilibration time of the initial electron distribution, which is indicative of the total thermalization process for the whole system, was reported to be 7 ps [1]. These studies, which have provided valuable insights, probe the SCOP dynamics through their effect on the electronic subsystem, i.e. the change in the initial electron temperature.

Direct observations of optical phonon dynamics were obtained through optical reflection studies that indicated the coherent nature of SCOP, with a decoherence time of 1–2 ps [11]. Time-resolved Raman spectroscopy [3, 12, 13] has also shown, by the direct probing of the population density of SCOP, that the decay time for the Γ – E_{2g2} phonon is 2 ps, close in value to the decoherence time. However, optical spectroscopy is sensitive to the center of the Brillouin zone (Γ region), where momentum conservation is fulfilled, thus limiting the information at, e.g., the K region. Moreover, equilibration pathways of the remaining phonon distribution are not known from SCOP decay. A comparison of the decay time of SCOP (1–2 ps) with the equilibration time constant of the electron temperature (7 ps) suggests that other important phonon–phonon relaxation processes are also involved and on different time scales. Theoretically, it was predicted that SCOP have a predominant decay channel not only to mid-frequency phonons, but also to acoustic phonons [14]. Such processes and time scales require a knowledge of structural changes with ultrafast spatiotemporal resolutions.

Here, we report on ultrafast electron crystallography (UEC) of nanoscale (1–3 nm thickness) graphite. The results elucidate the early non-equilibrium evolution of structural change due to optical phonons and the subsequent phonon decay from optically dark regions of the Brillouin zone. We resolve two elementary processes of 700 fs and 12 ps. UEC provides for the direct probing of the dynamics of structures [15] without being governed by optical selection rules. Previous experiments in our laboratory have focused on the electron reflection geometry of UEC, thus limiting it to the out-of-plane movements of atoms in graphite [16].

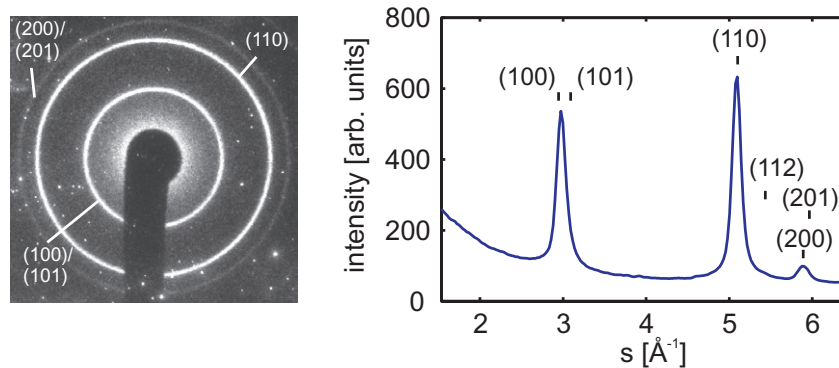


Figure 1. Diffraction pattern and the radially averaged peaks of graphite. The diffracted intensity at a scattering vector s is obtained by averaging the Debye–Scherer rings in the original diffraction pattern shown on the left. The indicated Bragg peak positions were calculated from a knowledge of the graphite unit cell dimensions.

Here, we use the transmission mode of UEC, which enables the probing of in-plane (lateral) movements of atoms. Transmission electron diffraction in perpendicular and tilted geometries provides for the probing of mechanical drumming of thin films of graphite [17, 18] and, as with x-ray diffraction [19] and absorption [20], direct information on atomic motions near melting can be obtained [21–23].

2. Experimental details

The experiments reported here were performed in Caltech’s UEC instrument, which has already been described in detail elsewhere [15, 24]. Briefly, ultrashort electron pulses are generated using a photoelectron source. The resulting electron packets are collimated and focused onto the sample by a magnetic lens system. The diffracted electrons are detected on a phosphor screen and recorded with a charge-coupled device. Structural dynamics are initiated by an ultrashort laser pulse (100 fs, 800 nm, 45° incidence angle, p -polarized, 1.5 mm spot size) and probed at different delay times Δt between the excitation laser pulse and the arrival time of the electron pulse at the sample. Typically, the probing pulse contains ~ 500 electrons. The fluence profile of the laser pulse was determined by scanning a knife edge across the laser beam while recording the residual laser power.

The sample is a graphite thin film with a thickness of 1–3 nm (Graphene Laboratories Inc.) mounted on a 2000-mesh grid. Since the grain size of the graphene single crystals is smaller than the size of the probing electron beam (100–200 μm), the diffraction pattern in transmission consists of the Debye–Scherer rings (see figure 1), but with some spots reflecting the existence of μm -sized grains. We note that in previous studies of the ultrafast dynamics of single crystals [16, 25], which employed a reflective diffraction geometry, the specular spot on the zero-order Laue ring was probed, thus investigating the dynamics of the first few nm resulting in diffraction spots and not streaks. This is comparable to the probed sample thickness in this transmission study. In previous studies [25], flatness and cleanness were checked by using scanning electron microscopy (SEM) and low-energy electron diffraction (LEED). It was found

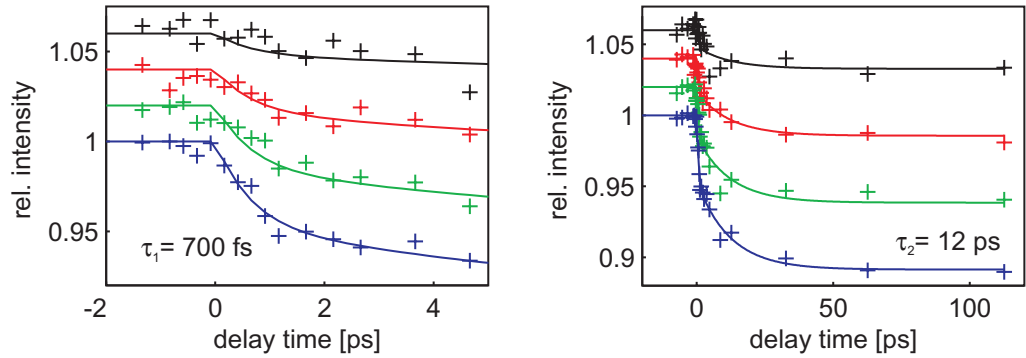


Figure 2. Intensity change in the (110) diffraction peak for ultrashort (left panel) and longer (right panel) delay times. After excitation with an absorbed fluence per layer of 18 (black), 35 (red), 53 (green) and 70 (blue) $\mu\text{J cm}^{-2}$, the intensity displays a drop with a time constant of 700 fs and an additional slower drop with a time constant of 12 ps, as obtained from the theoretical fits (see text). The relative magnitude of the 700 fs component to the total intensity drop is 45%.

that the probed surface area produced sharp LEED spots, and SEM indicated that no flakes are formed at the surface. Auger elemental analysis only showed a carbon signal, ruling out any substantial contamination of the surface.

To measure diffraction intensities at different delay times Δt , we radially averaged the ring pattern. The center of the diffraction ring in each pattern was determined by a Hough transform as used in image theory [26]. Each analyzed diffraction pattern was averaged over 10^4 single-shot frames, and for each delay time 30 patterns were recorded. An example of a radially averaged diffraction pattern is shown in figure 1, with the scattering vector defined as $s = 2k \sin(\theta)$, where $k = 2\pi/\lambda$ is the electron wave vector and 2θ the scattering angle. The expected positions of the Bragg peaks (hkl) are well reproduced. Only reflections with small l are observed, since the incident electron beam is perpendicular to the graphene plane. Care was taken to rule out the significance of any beam drift due to transient electric fields [25] (see the supplementary material, available from stacks.iop.org/NJP/13/063030/mmedia). For all the studies reported here, our focus is on diffraction intensity change and not on the position, because the lateral expansion of graphite is much smaller than interlayer expansion.

3. Results and discussion

In figure 2, we display the relative intensity change in the (110) Bragg peak at different delay times and for various absorbed fluences. The dynamics are characterized by two time scales, with one component being on the sub-ps time scale, and the other, slower, one being on a 10 ps time scale. By fitting a bi-exponential function, $I/I_0 = 1 - A[1 - \exp(-k_1 \Delta t)] - B[1 - \exp(-k_2 \Delta t)]$, to the experimental data points for the highest absorbed fluence per layer, $f = 70 \mu\text{J cm}^{-2}$ (corresponding to an incident fluence of 9.5 mJ cm^{-2}), we obtained the time constants $\tau_1 = 1/k_1 = 700 \text{ fs}$ and $\tau_2 = 1/k_2 = 12 \text{ ps}$. The relative magnitude of the intensity drop induced by the ultrafast process, $A/(A+B)$, is 0.45. Scaling the fit parameters A and B linearly with the fluence and keeping k_1 and k_2 constant provides good agreement for the fit with the experimental data for all fluences in the reported range. For delay times up to

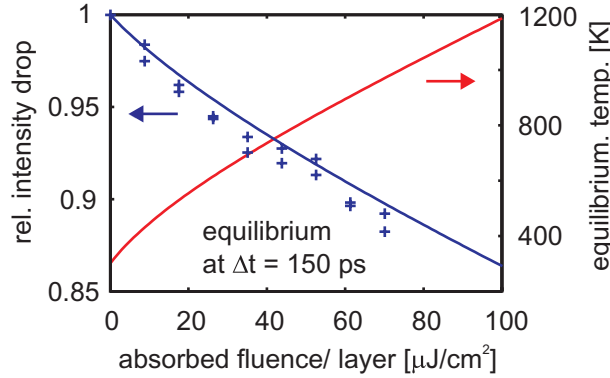


Figure 3. The experimentally observed diffraction and intensity change, together with calculated intensity at a longer time, $\Delta t = 150$ ps. The diffraction intensity drop at long delay times (blue crosses) can be well reproduced (without any adjustable parameter) by calculating the temperature rise (red curve) of graphite from the known optical and thermal material constants and using the Debye–Waller relation (blue curve). The nonlinearity shown is due to the temperature dependence of both the Debye–Waller factor and the heat capacity.

$\Delta t = 800$ ps (not shown), the diffracted intensity remains unchanged, indicating that there is no recovery by cooling, as expected for a thin film specimen and also consistent with the fact that transient electric fields are negligible at these fluences.

The time constant τ_2 of the picosecond process correlates with the equilibration time of the phonon distribution reported earlier from studies on the electron temperature [1]; see below. In order to unravel the nature of the femtosecond process, we first show in figure 3 that the intensity decrease at long delay times ($\Delta t = 150$ ps) is well described by an equilibrium heating model. For this purpose, we consider the temperature increase ΔT , as given by $f = \int_{T_0}^{T_0 + \Delta T} c_p dT$, where again f is the absorbed fluence per layer, c_p is the temperature-dependent heat capacity per unit area and layer of graphite, as taken from [27], and T_0 is the temperature of the thin film before laser excitation. The absorbed fluence per layer is given by $f = (c/2)F \cdot R/\alpha$, where F is the incident fluence and $c/2$ is the interlayer distance in graphite. The reflectivity $R = 0.27$ and the penetration depth $\alpha = 33$ nm of the excitation laser are calculated from the complex index of refraction [28]. The final temperatures, $T_0 + \Delta T$, for the range of utilized fluences are shown in figure 3 and are denoted by a red curve. For the highest fluence we obtained an equilibrium temperature increase of 700 K.

Given the value of ΔT we now can calculate the expected decrease in the diffracted intensity $I(T)$ in agreement with the Debye–Waller effect: $\log[I(T_0 + \Delta T)/I(T_0)] = 2[W(T_0) - W(T)]$. Because the in-plane Debye temperature ($\theta_D = 1300$ K; [29]) is significantly larger than the highest ΔT value, we can express $W(T)$ as

$$W(T) = \frac{\langle u_l^2 \rangle G^2}{4} = \frac{3\hbar^2 G^2}{2mk_b \theta_D} \left[\frac{1}{4} + \left(\frac{T}{\theta_D} \right)^2 \int_0^{\theta_D/T} \frac{s}{\exp(s) - 1} ds \right], \quad (1)$$

where m is the mass of the carbon atom, k_b is the Boltzmann constant and $\langle u_l^2 \rangle$ is the lateral atomic mean square displacement. The scattering vector is given by $G = 5.1 \text{ \AA}^{-1}$ for the (110)

Bragg spot. When the equilibrium is reached, e.g. at $\Delta t = 150$ ps, the predicted intensity decrease for different fluences is depicted in figure 3 (blue curve), together with the experimental results (crosses). Considering that no adjustable parameters were used, the agreement is very satisfactory.

Knowing that the structural description, and key parameters used, are valid in the equilibrium regime, we can then apply a generalized expression for $2W$ [30] that is appropriate for the femtosecond dynamics in the non-equilibrium regime:

$$2W = \frac{1}{2} \sum_{g,j} (G \cdot e_{g,j})^2 \langle a_{g,j}^2 \rangle. \quad (2)$$

Here, the summation is over all phonon branches j and phonon wave vectors g . The polarization of the (g, j) -phonon is denoted by $e_{g,j}$ and $\langle a_{g,j}^2 \rangle$ is the mean square amplitude for a particular phonon of the lattice. The mean square amplitude of a phonon is connected (in the classical limit) to its average energy per atom, $\langle E_{g,j} \rangle / N$, by

$$\langle a_{g,j}^2 \rangle = \frac{2\langle E_{g,j} \rangle / N}{m\omega_{g,j}^2}, \quad (3)$$

where $\omega_{g,j}$ is the frequency of the phonon. The fact that the displacement is inversely proportional to the phonon frequency excludes the influence of SCOP on the decrease in diffracted intensity.

The SCOP have frequencies of 300 THz ($\Gamma-E_{2g2}$) and 260 THz ($K-A'_1$), and even if we take the whole excitation energy to be stored in the SCOP mode, representing an upper limit, we obtained for $f = 70 \mu\text{J cm}^{-2}$ (corresponding to $0.12 \text{ eV atom}^{-1}$) a mean-square amplitude of 25 pm^2 ; by symmetry, $(G \cdot e_{g,j})^2$ equals $G^2/2$. From equation (2) this value translates into a maximum SCOP-induced intensity drop of the diffraction peak of only 1.6%, contrary to the experimentally observed $\sim 5\%$ of the initial component (see figure 2). Due to their high frequency and correspondingly small mean-square amplitudes, electron diffraction in this configuration is insensitive to map the initial excitation of the SCOP, and the observed 700 fs component cannot be due to their effect on the structure.

A recent theoretical study of the phonon decay pathways in graphite [14] has given a more complete picture to compare with. In this picture, a SCOP decay involves a ‘three-particle’ interaction, a process that leads to two phonons from the original SCOP in agreement with conservation of the total energy and momentum (figure 4). This process leads to well-defined decay paths for the SCOP. As shown in figure 4, both the $\Gamma-E_{2g2}$ and the $K-A'_1$ phonons (with 100% and $\sim 50\%$ probability, respectively [14]) decay to other phonons of frequency around 150 THz (green stripe) and with polarization vectors, $e_{g,j}$, predominantly ($\sim 95\%$; [14]) within the graphene plane. The $K-A'_1$ phonons have an additional decay channel with a probability of $\sim 50\%$ to low-frequency, in-plane acoustic phonons having $\omega \sim 20 \text{ THz}$ [14].

We first consider the influence of the mid-frequency phonons on the diffraction intensity. When the excitation energy is transferred to these modes we obtain a 6.4% intensity decrease, in close agreement with our experimental results of $\sim 5\%$ for the 700 fs process; thus we assign it to the decay mechanism that we depict in figure 4 for the different regions of the Brillouin zone. Considering that the $K-A'_1$ and $\Gamma-E_{2g2}$ SCOP are initially equally populated [32], the predicted acoustic decay channel of the $K-A'_1$ phonon would lead to an intensity decrease with a total change of 12%, which is significantly larger than the observed diffraction intensity change. However, the relative population of the $K-A'_1$ and $\Gamma-E_{2g2}$ SCOP is set by the interplay of

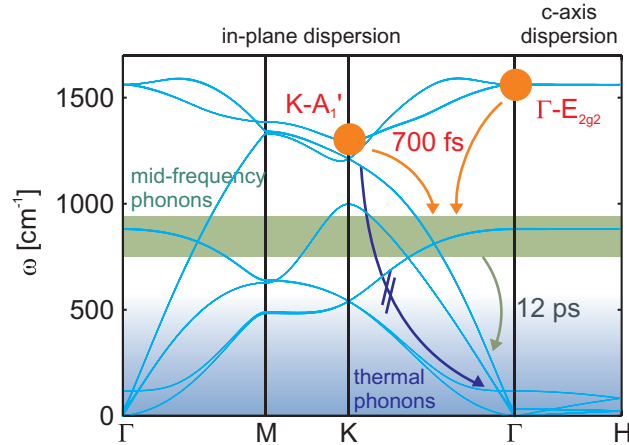


Figure 4. Graphite phonon band structure and equilibration mechanism. Shown here are the two primary processes we observe in the structural dynamics using UEC. The SCOP $\Gamma-E_{2g2}$ and $K-A'_1$ (orange circles) decay to mid-frequency phonons with a time constant τ of 700 fs, which subsequently equilibrate with the remaining lattice with a time constant of 12 ps. The predicted emission of acoustic phonons (blue arrow) is not observed. The dispersion relation is taken from [31] ($\Gamma-H$ distance not to scale).

early inter- and intra-valley electron scattering processes [32] and depends on the amount of excitation. Our results indicate that, at the fluence range employed here, either the population of $K-A'_1$ phonons is negligible or the emission of acoustic phonons is less effective than was predicted previously.

The time constant for the population of the mid-frequency phonons (700 fs) reported here is smaller than the previously reported time constant for the decay of the $\Gamma-E_{2g2}$ SCOP (~ 2 ps) [12]. However, the temperature of the specimen has some effect on the rate of relaxation. It was recently shown by time-dependent Raman spectroscopy [13] that the decay time of the $\Gamma-E_{2g2}$ phonon shows a strong temperature dependence that leads to a decay time in the range of 1–1.5 ps for samples that were heated to 600 K. A similar trend can be inferred from the increase in Raman line width in static experiments, where the sample was excited by a high electric current [3], although part of this broadening might be attributed to inhomogeneous excitation [8]. At the fluence used here we therefore expect the decay to be nearly 1 ps, as reported in this paper. An interesting question for future studies is the following: if the initial nuclear motion is nearly confined to in-plane displacements, how can graphite expand along the c -axis on the ultrashort time scale (see [16, 21, 25])? The potential energy interaction could drive expansions [33] and even contractions, as reported theoretically [34] and experimentally [16, 21, 25], and the overall dynamics will then be controlled by the relative time scales involved in the nuclear motions and in the potential change of the lattice.

4. Conclusion

In conclusion, using UEC we have shown that the atomic mean-square displacement in nanoscale graphite exhibits a bi-exponential structural dynamics behavior with time constants (700 fs and 12 ps) characteristic of different modes of the lattice and regions in the Brillouin

zone. The observed diffraction intensity change, when compared with the results of a more complete theoretical model of atomic motions, identifies the primary component of structural dynamics: the emission of mid-frequency phonons generated from the decay of strongly coupled, optical phonons to spectroscopically inaccessible, optically dark regions of the Brillouin zone. The slower 12 ps component represents the increased atomic mean-square displacement of a heated lattice, which we examined at different fluences to establish that the equilibrium state is reached. Such studies elucidate the initial local distortion of the unit cells and the non-equilibrium primary dynamics of the structure.

Acknowledgments

This work was supported by the National Science Foundation and the Air Force Office of Scientific Research in the Center for Physical Biology at Caltech supported by the Gordon and Betty Moore Foundation. One of the authors (SS) gratefully acknowledges a scholarship from the Alexander von Humboldt Foundation.

References

- [1] Kampfrath T, Perfetti L, Schapper F, Frischkorn C and Wolf M 2005 *Phys. Rev. Lett.* **95** 187403
- [2] Maultzsch J, Reich S, Thomsen C, Requardt H and Ordejón P 2004 *Phys. Rev. Lett.* **92** 075501
- [3] Berciaud S, Han M Y, Mak K F, Brus L E, Kim P and Heinz T F 2010 *Phys. Rev. Lett.* **104** 227401
- [4] Barreiro A, Lazzeri M, Moser J, Mauri F and Bachtold A 2009 *Phys. Rev. Lett.* **103** 076601
- [5] Steiner M, Freitag M, Perebeinos V, Tsang J C, Small J P, Kinoshita M, Yuan D, Liu J and Avouris P 2009 *Nat. Nano* **4** 320320
- [6] Breusing M, Ropers C and Elsaesser T 2009 *Phys. Rev. Lett.* **102** 086809
- [7] Neugebauer P, Orlita M, Faugeras C, Barra A L and Potemski M 2009 *Phys. Rev. Lett.* **103** 136403
- [8] Huang L, Hartland G V, Chu L Q, Luxmi Feenstra R M, Lian C, Tahy K and Xing H 2010 *Nano. Lett.* **10** 1308–13
- [9] Wang H *et al* 2010 *Appl. Phys. Lett.* **96** 081917
- [10] Lui C H, Mak K F, Shan J and Heinz T F 2010 *Phys. Rev. Lett.* **105** 127404
- [11] Ishioka K, Hase M, Kitajima M, Wirtz L, Rubio A and Petek H 2008 *Phys. Rev. B* **77** 121402
- [12] Yan H, Song D, Mak K F, Chatzakis I, Maultzsch J and Heinz T F 2009 *Phys. Rev. B* **80** 121403
- [13] Kang K, Abdula D, Cahill D G and Shim M 2010 *Phys. Rev. B* **81** 165405
- [14] Bonini N, Lazzeri M, Marzari N and Mauri F 2007 *Phys. Rev. Lett.* **99** 176802
- [15] Zewail A H and Thomas J M 2010 *4D Electron Microscopy: Imaging in Space and Time* (London: Imperial College Press)
- [16] Carbone F, Baum P, Rudolf P and Zewail A H 2008 *Phys. Rev. Lett.* **100** 035501
- [17] Kwon O H, Barwick B, Park H S, Baskin J S and Zewail A H 2008 *Nano Lett.* **8** 3557–62
- [18] Park H S, Baskin J S, Barwick B, Kwon O H and Zewail A H 2009 *Ultramicroscopy* **110** 7–19
- [19] Lindenberg A M *et al* 2005 *Science* **308** 392–5
- [20] Chergui M 2010 *Acta Crystallogr. Sect. A* **66** 229–39
- [21] Raman R K, Murooka Y, Ruan C Y, Yang T, Berber S and Tomanek D 2008 *Phys. Rev. Lett.* **101** 077401
- [22] Nie S, Wang X, Park H, Clinite R and Cao J 2006 *Phys. Rev. Lett.* **96** 025901
- [23] Siwick B J, Dwyer J R, Jordan R E and Miller R J D 2003 *Science* **302** 1382–5
- [24] Ruan C Y, Vigliotti F, Lobastov V A, Chen S and Zewail A H 2004 *Proc. Natl Acad. Sci.* **101** 1123–8
- [25] Schäfer S, Liang W and Zewail A H 2010 *Chem. Phys. Lett.* **493** 11–18
- [26] Illingworth J and Kittler J 1988 *Comput. Vis. Graph. Image Process.* **44** 87–116
- [27] Butland A and Maddison R 1973 *J. Nucl. Mater.* **49** 45–56

- [28] Palik E D (ed) 1991 *Handbook of Optical Constants of Solids II* (New York: Academic)
- [29] Chen R and Trucano P 1978 *Acta Crystallogr. A* **34** 979–82
- [30] Warren B E 1990 *X-Ray Diffraction* (New York: Dover)
- [31] Wirtz L and Rubio A 2004 *Solid State Commun.* **131** 141–52
- [32] Butscher S, Milde F, Hirtschulz M, Malić E and Knorr A 2007 *Appl. Phys. Lett.* **91** 203103
- [33] Yang D S, Gedik N and Zewail A H 2007 *J. Phys. Chem. C* **111** 4889–919
- [34] Jeschke H O, Garcia M E and Bennemann K H 2001 *Phys. Rev. Lett.* **87** 015003